Chapter 10
Inversion Methodology of Ground Level Enhancements

B. Heber, N. Agueda, R. Bütikofer, D. Galsdorf, K. Herbst, P. Kühl, J. Labrenz, and R. Vainio

Abstract While it is believed that the acceleration of Solar Energetic Particles (SEPs) is powered by the release of magnetic energy at the Sun, the nature, and location of the acceleration are uncertain, i.e. the origin of the highest energy particles is heavily debated. Information about the highest energy SEPs relies on observations by ground-based Neutron Monitors (NMs). SEPs with energies above 500 MeV entering the Earth's atmosphere will lead to an increase of the intensities recorded by NMs on the ground, also known as Ground Level Event or Ground Level Enhancement (GLE). A Fokker-Planck equation well describes the interplanetary transport of near relativistic electrons and protons. An NM is an integral counter defined by its yield function. From the observations of the NM network, the additional solar cosmic ray characteristics (intensity, spectrum, and anisotropy) in the energy range $\gtrsim 500$ MeV can be assessed. If the interplanetary magnetic field outside the Earth magnetosphere is known (see Sect. 10.3.2) a computation chain can be set up in order to calculate the count rate increase of an NM for a delta injection at the Sun along the magnetic field line that connects the Sun with the Earth (Sect. 10.3.3). By this computations, we define a set of

B. Heber (✉) • D. Galsdorf • K. Herbst • P. Kühl • J. Labrenz
Christian-Albrechts-Universität zu Kiel, Kiel, Germany
e-mail: heber@physik.uni-kiel.de; galsdorf@physik.uni-kiel.de; herbst@physik.uni-kiel.de; kuehl@physik.uni-kiel.de; labrenz@physik.uni-kiel.de

N. Agueda
University of Barcelona, Barcelona, Spain
e-mail: agueda@fqa.ub.edu

R. Bütikofer
University of Bern, Physikalisches Institut, Sidlerstrasse 5, CH-3012 Bern, Switzerland

High Altitude Research Stations Jungfraujoch and Gornergrat, Sidlerstrasse 5, CH-3012 Bern, Switzerland
e-mail: rolf.buetikofer@space.unibe.ch

R. Vainio
Department of Physics and Astronomy, University of Turku, Turku, Finland
e-mail: rami.vainio@utu.fi

Green's functions that can be fitted to an observed GLE to determine the injection time profile. If the latter is compared to remote sensing measurements like radio observations, conclusions of the most probable acceleration process can be drawn.

10.1 Introduction

The Earth is constantly bombarded by high-energy particles, also known as cosmic rays. Those who are not deflected by the geomagnetic field, as discussed in Chap. 5, enter the atmosphere and undergo interactions with atoms and molecules as well as with the nuclei of the atmosphere. Low-energy cosmic rays (<500 MeV) are absorbed in the atmosphere, i.e. no secondary particles can be observed at sea level from primary particles as described in Chap. 6. Most of the primary particles are of galactic origin and are known as Galactic Cosmic Rays (GCR). In solar eruptive events, such as solar flares and Coronal Mass Ejections (CMEs), protons and other ions can be accelerated to high energies (>30 MeV). The acceleration mechanisms are thought to be related to magnetic reconnection in solar flares (Aschwanden 2012) and the shock waves generated by CME (Cliver et al. 2004).

According to the review by Reames (1999) impulsive events are small, electron rich, tend to be enriched in heavy ions and are ^{3}He-rich (^{3}He/^{4}He≈1). They are associated with small magnetic loops in the lower corona with heights smaller than 10^4 km and have ionization states typical of solar flare temperatures, i.e., 10^7 K (Mason 2007). The emission is generated at low altitudes, and fast drift (type III) radio emission, which reflects the electron escape into the interplanetary medium (Klein and Trottet 2001), is observed as well.

Gradual SEP events, in contrast, are believed to originate high in the corona from a CME-driven shock whose extent is consistent with the observations of such SEP over relatively wide longitudinal ranges (Rouillard et al. 2011; Dresing et al. 2014). The association of CMEs with type II emission (see Chaps. 1 and 2 for details) also confirms the conclusion that gradual SEP events are accelerated by large CME-driven shocks (Reames 1999). These events produce some of the highest intensity events observed at Earth at energies up to several GeV (Mewaldt et al. 2012; Kühl et al. 2016).

While this two class picture appears to describe the origin of <50 MeV ions with some success, the origin of SEPs that cause GLEs is less studied due to the lack of detailed observations (Moraal and McCracken 2012). It was found that the GLE spectra tend to be slightly harder than non-GLE spectra and that they are consistent with double power laws (Mewaldt et al. 2012; Kühl et al. 2016). Also, the authors found that the composition of GLEs tends to have higher Fe/O ratios, enrichments in ^{3}He (Wiedenbeck 2013) and highly-ionized charge-states of heavy elements such as Fe. This lead to the conclusion that GLE ions may be accelerated by CME-driven shocks, with quasi-perpendicular shock geometry and the presence of suprathermal ions from previous flares playing a key role (Tylka et al. 2005). Moraal and Caballero-Lopez (2014) found different scenarios for different GLEs

having a prompt component from the impulsive phase and a gradual one indicating shock acceleration. To gain further insight the interplanetary and magnetospheric transport of high energy charged particles needs modeling (Bieber et al. 2004). While a Fokker-Planck equation well describes the interplanetary transport of near relativistic electrons (Dröge 2003; Dröge et al. 2010) the processes that need to be included at high energies have not been fully explored (Dalla et al. 2013, 2015).

Gradual particle events tend to be larger, typically associated with large 10^5 km X-ray emitting structures, last much longer than impulsive events, are proton-rich without significant enrichment in ^{3}He/^{4}He, electron poor, and have elemental abundances and charge states representative of solar coronal or solar wind material and temperatures, i.e., 10^6 K (Klecker 2013).

However, the relative roles of both components and how we can discriminate them remains a key problem in solar and solar-terrestrial physics, especially regarding the diverse interest in GLEs. There is a practical interest in GLEs owing to their significance for space weather. Solar cosmic rays can damage spacecraft electronic components and are a significant radiation hazard to astronauts. To quantify these risks, the full particle distribution in energy and pitch angle as a function of time needs to be determined from the NM observations. A method to derive the "physical quantities" is based on forward-modeling of SEP transport (Sects. 10.3.1 and 10.3.2) in interplanetary space and the Earth's magnetosphere (see also Chaps. 4 and 5) by utilizing a power law spectrum in rigidity at the injection point of the Sun (see Chap. 3) and the response/yield function of the NM (see Sect. 10.3.2 and Chap. 6). The forward modeling is utilized in Sect. 10.4 to derive an inversion methodology that is applied to observations in Sect. 10.5. To validate our model chain, results are compared to spacecraft measurements that are described in Sect. 10.2.

10.2   Space and Ground Based Measurements of GLEs

SEP events, where protons are accelerated to energies above 500 MeV, occur a few times per solar cycle. Protons with such energies penetrate the Earth's atmosphere and produce secondary particle showers which can increase the intensities recorded by NMs on the ground. Such intense SEP events are also known as Ground Level Events or GLEs. Initially designed by Simpson (1948), NMs are used for precise monitoring of spectral and directional variations in the cosmic-ray flux. The detection of a GLE event by an NM on average occurs a few times per solar cycle. The first GLE was observed on February 28, 1942 and the first GLE observed by NMs was the one on February 23, 1956 (see gle.oulu.fi).

Since 1942 until the end of 2015 a total of about 70 GLEs have been observed, i.e. ∼one GLE per year. Each GLE has its typical characteristics (amplitude, spectrum, duration, spatial distribution of flux, etc.). During a GLE the measurements of the ground-based NM network show an increase in the count rate within typically a few minutes and decreasing intensities to background levels within hours. In some

cases, GLEs show a double-peaked time structure, with an initial fast rise and an anisotropic particle population—called "prompt component"—followed by a more gradual and less anisotropic "delayed component" (McCracken et al. 2012).

SEP events causing GLEs are restricted to events that accelerate ions to energies above ∼500 MeV/nucleon. Experiments on board spacecraft located close to Earth such as the Geostationary Operational Environmental Satellites (GOES), the Solar and Heliospheric Observatory (SOHO), the Payload for Antimatter Matter Exploration and Light-nuclei Astrophysics (PAMELA) and the Alpha Magnetic Spectrometer 02 (AMS-02) aboard the International Space Station (ISS) can observe protons below and above this threshold in differential energy channels. These data serve to fill an observational gap between the few hundred MeV and less, typically monitored by other satellite instruments on board e.g. the Advanced Composition Explorer (ACE) (Gold et al. 1998) and Wind (Lin et al. 1995). This latter spacecraft allows us to determine the chemical and isotope abundance (Mewaldt et al. 2007; Nitta et al. 2015), the charge states (Mason et al. 1995; Kartavykh et al. 2007) and to study the lepton component i.e. electrons (Dröge 2000; Dresing et al. 2012, 2014; Agueda et al. 2014) during SEP events. As discussed in Chap. 4 it is important to know not only the intensity-time profiles but also the evolution of the PAD. The pitch angle is defined as the angle between the magnetic field and the velocity vector β. A particle instrument with a limited opening angle and a pointing direction **n** in interplanetary space is sensitive to a pitch angle range around $\cos(\vartheta) = -\frac{\mathbf{B} \cdot \mathbf{n}}{B}$ with **B** the interplanetary magnetic field vector. Spacecraft like ACE, Wind, and the International Monitoring Platform (IMP) 8 outside the Earth's magnetosphere provide us with measurements of the interplanetary magnetic field vector **B** near the first Lagrangian point L1. Contrary to IMP 8 neither GOES nor SOHO measures **B**. The OMNI dataset[1] maintained by the US National Space Science Data Center provides us with the magnetic field, and plasma data sets from ACE, Wind and the IMP-8 shifted to the Earth's bow shock nose. For an observer in the magnetosphere, (PAMELA and AMS-02) the viewing direction **n** is the asymptotic direction that has to be calculated as described in Chap. 5.

10.2.1 dE/dx-dE/dx-Method

This method is utilized by EPHIN aboard SOHO and is based on the energy loss in two detectors. Figure 10.1 right illustrates the measurement principle of the EPHIN instrument (Müller-Mellin et al. 1995). Plotting the energy loss in two
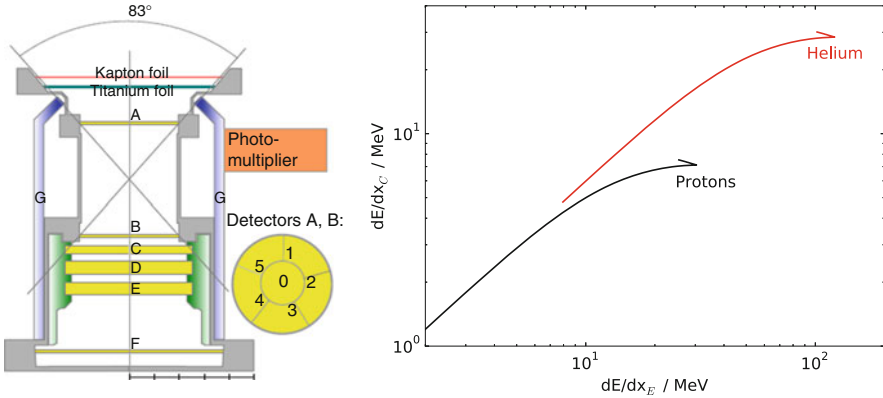
---

[1]http://omniweb.gsfc.nasa.gov/owmin.html.

Fig. 10.1 The *left and right panels* display a sketch of the Electron Proton Helium INstrument (EPHIN) aboard SOHO (Müller-Mellin et al. 1995) and the dE/dx-dE/dx measurement principle applied to it, respectively

adjacent detectors against each other, the mean energy losses of H and He follow the characteristic tracks. This is used to identify the particle species in certain areas of the two-dimensional pulse height plane. In these regions, the energy loss in both detectors is attributed to the incoming energy of the particle. Both Goddard Medium Energy (GME) experiment and the Medium Energy Detector (MED) (Meyer and Evenson 1978) utilize this technique.

EPHIN is a multi-element array of solid state detectors with anticoincidence to measure energy spectra of electrons in the range 250 keV to >8.7 MeV, and of hydrogen and helium isotopes in the range 4 MeV/n to >53 MeV/n. The instrument is sketched in Fig. 10.1 left and consists of a stack of silicon solid state detectors (A-F) surrounded by an anticoincidence (scintillator, G). The method to derive energy spectra for penetrating particles with energies above 50 MeV/nucleon is described in detail by Kühl et al. (2015). Since relativistic protons and electrons have the same energy loss dE/dx in matter, electrons with energies above 10 MeV are leading to too high fluxes at energies above ≈ 700 MeV for protons when utilizing the $dE/dx - dE/dx$-method.

The second instrument utilizing this method is the GME aboard IMP-8 that was launched by NASA in 1973 into a 35 R_E geocentric orbit with a 12 days period. The spacecraft was in the solar wind for 7–8 days of every 12-day orbit, where it measured the magnetic fields, plasma, and energetic charged particles (e.g., cosmic rays). The spacecraft spin axis was normal to the ecliptic plane, and the spin rate was 23 rpm. PAD information was obtained in eight angular sectors.

In contrast to EPHIN, the MED design consisted of three pulse-height analyzed CsI detectors with thicknesses of 1 mm, 2 cm and 1 mm, respectively, and a cylindrical plastic scintillator anticoincidence shield. Penetrating particles have an energy above 80 MeV and a geometry factor of nearly 5.0 cm^{2}sr (for details see http://spdf.gsfc.nasa.gov/imp8_GME/GME_instrument.html).

10.2.2   dE/dx - C

This method is used for penetrating particles. This method is based on charged particles completely penetrating the Solid State Detector (SSD) and a Cerenkov detector (C), which is placed underneath. If the particles penetrate C faster than with the speed of light in this medium, i.e., with a speed of $\beta > \frac{1}{n}$ where n is the refractive index of the material, they produce a measurable light flash (Cerenkov radiation). Plotting the Cerenkov detector signal against the energy-loss by ionization, ΔE in the SSD results in characteristic curves for protons and helium, clearly separated with their slopes depending on particle speed. Thus, the method allows an identification of the penetrating particles and gives their energy above a threshold speed. This method is utilized by the HEPAD assembly (Rinehart 1978) aboard a series of GOES satellites in geosynchronous orbit maintained by National Oceanic and Atmospheric Administration (NOAA), which provides differential fluxes in three channels between 350 MeV and 700 MeV, and integral flux above 700 MeV (Sauer 1993). HEPAD consists of two 500 μm thick silicon detectors and a silica radiator. The two surface barrier silicon detectors have an area of 3 cm^2 and define an effective acceptance aperture of ∼24° half-angle.

Charged particles, which completely penetrate the two semiconductor detectors, can be studied with the help of the Cerenkov-detector (McDonald 1956; Linsley 1955), which is placed underneath the semiconductor detectors. The use of a different detector is necessary since, with energy-loss-measurements alone, the energy determination is only possible in a narrow energy range above the maximum energy for stopping particles. The official archive for GOES Energetic Particle data, including proton flux data, can be found at the National Geophysical Data Center.[2]

10.2.3   Magnet Spectrometer

In addition we utilize data from the Russian-Italian PAMELA mission (Picozza et al. 2007) and the AMS-02 aboard the ISS (Aguilar et al. 2013; Kounine 2012). PAMELA as well as AMS-02 are magnetic spectrometers in Low Earth Orbit, providing extremely high-quality observations of electrons and ions, which we have used for validation and cross-calibration purposes. Because the orbits of PAMELA and AMS are within the Earth's magnetic field, the two spacecraft do not have a 100% duty cycle for observing low-energy cosmic rays (Adriani et al. 2011). Therefore our approach is to use their observations to validate measurements e.g. from EPHIN.

---

[2]http://www.ngdc.noaa.gov/stp/satellite/goes/.

10.3   Forward Modeling from the Sun to the Observer at Ground

The project HESPERIA gathered experts in different fields to take into account interconnections between the solar, heliospheric and NM communities and to advance our knowledge of GLEs further. The group developed a model chain allowing to infer the solar release time profile of relativistic SEPs and their interplanetary transport parameters directly from NM observations. The process chain starts with the propagation of SEPs from the Sun to the Earth. Utilizing the local interplanetary field in Geocentric Solar Ecliptic (GSE) coordinates, the PAD outside the magnetosphere can be converted to an angular distribution in GSE coordinates. Computing the energetic particle transport in the geomagnetic field and taking into account the NM yield function the count rate variation of all NMs that have measured the event can be predicted. Although the physics of the underlying processes is discussed in detail in Chap. 4 (interplanetary transport), Chap. 5 (transport through the magnetosphere) and Chap. 6 (ground-based measurements by NMs) we will show in a compact way how the different models need to be interlinked.

10.3.1   Interplanetary Particle Transport: From the Sun to the Magnetosphere

Here we give a summary of Chap. 4 in which we model the particle transport from the Sun ($r_i = 2\ r_{Sun}$) in an unperturbed solar wind with constant velocity v. The Interplanetary Magnetic Field (IMF) can be described as a smooth average field, represented by an Archimedean spiral, with superposed magnetic fluctuations. The quantitative treatment of the evolution of the particle's phase space density, $f(z, \mu, t)$, can be described by the focused transport equation (Roelof 1969):

$$\frac{\partial f}{\partial t} + \beta c\, \mu \frac{\partial f}{\partial z} + \frac{1 - \mu^2}{2L} \beta c\, \frac{\partial f}{\partial \mu} - \frac{\partial}{\partial \mu} \left(D_{\mu\mu} \frac{\partial f}{\partial \mu} \right) = q(z, \mu, t) \tag{10.1}$$

Here z is the distance along the magnetic field line that depends on the solar wind velocity v, $\mu = \cos \alpha$, is the cosine of the particle pitch angle, α, and t is the time. The systematic force is characterized by the focusing length, $L(z) = -B(z)/(\partial B/\partial z)$, in the diverging magnetic field B, while the stochastic forces are described by the pitch-angle diffusion coefficient $D_{\mu\mu}(\mu)$. As discussed in detail in Chap. 4 the pitch-angle diffusion coefficient has the same form as in Agueda et al. (2008).

Another approximation was introduced by Hasselmann and Wibberenz (1970). If we take the particle radial mean free path, λ_r, to be spatially constant, then the mean free path parallel to the IMF line is given by $\lambda_{||} = \lambda_r \sec^2 \psi$, where ψ is the angle

between the field line and the radial direction. As shown in Chap. 4 it is sufficient to compute a database of "Green's-functions" for particles moving with the speed of light ($\beta = 1$). The database consists of 30 different values of the radial mean free path, from $\lambda_r = 0.1$ to $\lambda_r = 2.0$ AU and for solar wind velocities ranging from 300 to 700 km/s. The intensity spectra at the source are given by the solar spectrum that is typically a power-law with $N(R) \propto R^{-\gamma}$, where γ is the spectral index of the solar source. Results of this modeling have been discussed in Chap. 4 and (Agueda 2008). There the results could be directly compared to spacecraft measurements. However, observations in the magnetosphere and ground-based measurements need to take into account the geomagnetic filter as described in Chap. 5 and the shielding by the atmosphere and the specific response of the NM (Chap. 6).

If we assume for each energy interval a **number of delta injections** in time at the source region the phase space density $f(z, \mu, t)$ can be calculated for any time t at 1 AU corresponding to a distance $z(v)$ depending on the solar wind velocity v for every μ if the **mean free path λ_r**, the solar wind speed v and the direction of the interplanetary magnetic field are known. Acceleration theories (see Chap. 3), as well as measurements, suggests that the source spectrum is given by a power law described by the **spectral index γ**. **Thus three free parameters describe the temporal evolution of a SEP event caused by a single δ-injection at the Sun.**

10.3.2 *From the Interplanetary Particle Distribution to Neutron Monitor Measurements - Magneto- and Atmospheric Transport of Charged Energetic Particles*

The transport of cosmic ray particles in the geomagnetic field and in the Earth's atmosphere are described in detail in the Chaps. 5 and 6. Here we refer to the objects that are relevant to the investigations of NM data during solar cosmic ray events. The asymptotic viewing directions for each NM station are often computed only for primary cosmic ray particles that penetrate into the Earth's atmosphere from a vertical direction. The contribution of obliquely incident particles is often neglected in GLE analysis as their contribution to the counting rate is assumed to be small because of the soft spectrum of the solar cosmic rays.

The minimum rigidity that a charged energetic particle must have to reach a location within the magnetosphere and from a given direction of incidence is expressed by the geomagnetic cutoff rigidity R_C. This cutoff rigidity varies from a minimum at the magnetic poles ($R_C \approx 0$ GV) to a value of about 15 GV in equatorial regions. The asymptotic direction for a NM, for a given direction of incidence into the Earth's atmosphere above the location of the NM and a selected

particle rigidity, is defined as the direction of motion of the primary cosmic ray particle before penetrating the Earth's magnetosphere. In contrast to previous work by e.g. Bieber et al. (2004), neither the shape of the PAD nor the incoming direction is a free parameter in the High Energy Solar Particle Events forecasting and Analysis (HESPERIA) approach. The PAD of SEPs outside the Earth's magnetosphere is calculated as described in Sect. 10.3.1. To assign for each rigidity the pitch angle range of a NM we need to know the Interplanetary Magnetic Field (IMF) direction close to the Earth magnetopause and the asymptotic direction in GSE coordinates. In HESPERIA, we make use of the 5-min averaged OMNI data to prepare a set of magnetic field directions outside the magnetosphere, to be used as the directions of the symmetry axis of the directional relativistic proton distribution. The field to which the distribution tends to become gyro-tropic is not the momentarily measured field at the particle position but rather the field it averages over. Although the timescales of the gyro motion are relatively small, the spatial ones are not. A first order estimation, $r_L/(u_{SW}t) \sim 1$, leads to $t = 1670\,$s for the averaging time of the fluctuating field for a 1-GV particle in a 5 nT field and a solar wind speed of 400 km/s. However, it should be noted that particles would need a rigidity-dependent averaging time of the field direction. As an example, Fig. 10.2 displays on the left the rigidity-dependent vertical asymptotic directions for a stationary observer in Kiel from 1:30 to 3:00 UT on May 17, 2012. The colored triangles show the direction of the interplanetary field for each period. From these two directions, the pitch angle for each rigidity and time can be calculated. The right panel of Fig. 10.2 displays the corresponding results.
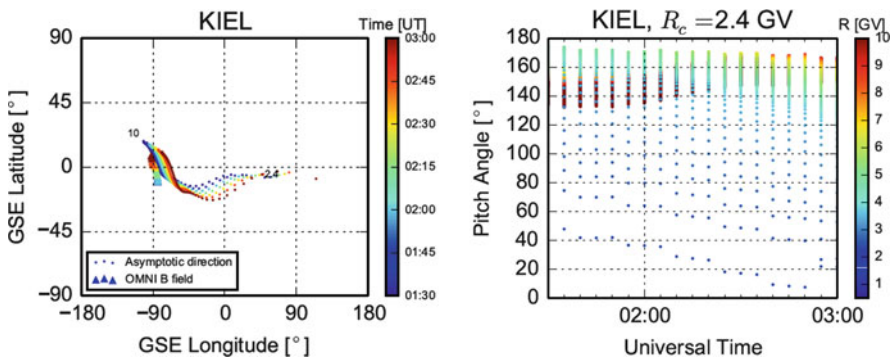

Fig. 10.2 *Left*: Calculations of the asymptotic direction at different rigidities during the onset of the May 17, 2012 SEP event as function of time for an observer at Kiel. The *triangles* indicate the direction of the interplanetary magnetic field. The *right panel* shows the pitch angle coverage for the same period. For details see text

If we assume that only protons are accelerated in a SEP event to sufficient rigidities R that NMs can measure, then the count rate N caused by solar cosmic ray protons at the NM station x and at time t can be expressed by:

$$N_x(t) = \int_{R_c}^{R_u} I(R, \alpha, t) \cdot S_x(R, h) \cdot dR, \tag{10.2}$$

where R_c and R_u are the cutoff and upper ($R_u = 20$ GV) rigidities, α the pitch angle of the incoming proton, $S_x(R, h)$ the yield function of the NM station x at the atmospheric depth, h (for details see Chap. 6). Here Eq. (10.2) is approximated by the sum of discrete values covering the full rigidity and pitch angle range. The upper value of $R_u = 20$ GV was chosen because there is no observational evidence for SEP protons with rigidities above 20 GV.

> Given the IMF vector **B** in GSE coordinates and the asymptotic directions **n** in the same coordinate system, we compute the pitch angle, α coverage, for each NM. Together with the yield function described in Chap. 6 the count rate increase for each NM is computed.

10.3.3   Combined Greens-Function

As part of HESPERIA, the two models described in the previous two sections were combined. The first step is to compute the additional count rate, N, caused by SEPs for a given NM station with cutoff rigidity R_C at the time t_1, based on the computed rigidity and cosine of the pitch angle (μ) dependent intensity $I_1(\mu, t_1, r)$ of relativistic protons at time t_1. This spectrum I_1 results from an energy spectrum $I_0 \propto R^{-\gamma}$ injected as a δ-function at a time t_0 before t_1. The two parameters determining the injection function are the power-law index γ and the number of particles injected at a rigidity $R = 1$ GV. The particle transport in the IMF is described by Eq. (10.1) using λ_0 as the only free parameter. The path length of the particles is determined by the solar wind speed measured at 1 AU (see Sect. 10.3.1). The IMF outside the Earth's magnetosphere together with the asymptotic direction calculated for t_1 gives the pitch angle coverage for the NM. Within HESPERIA the Green's function $G_\beta(t, z, \mu, v)$ are derived from the ones $G_c(t, z, \mu, c)$ that are available from SEPServer (http://server.sepserver.eu) for relativistic protons ($\beta = 1$). For near relativistic particles the energy loss in the IMF can be neglected and therefore the Green's function for a lower velocity β is given by:

$$G_\beta \left(\frac{1}{\beta} t, z, \mu, \beta \right) = \beta G_c(t, z, \mu, c) . \tag{10.3}$$

We consider near relativistic protons with rigidities from 0.5 to 20 GV (kinetic energies from 0.12 to 19 GeV) and following a power law in rigidity $I(R) = I_0 \cdot R^{-\gamma}$ with the spectral index γ.

The proton mean-free path is taken to increase with rigidity following the standard model. The resulting pitch angle dependent energy spectra at 1 AU are transported through the magnetosphere and atmosphere as described above.

10.4 Inversion Methodology

The previous two sections are describing the forward modeling of energetic particles from the Sun through the inner helio-, magneto- and atmosphere. Up to now, the inversion has only been attempted in two separate steps:

Inversion of NM data: The standard analysis of GLE events is based on solving an inverse problem where data by the worldwide network of NMs is used to determine the spectral and angular characteristics of SEPs near Earth but outside the magnetosphere causing the GLE.

Inversion of spacecraft data: The injection time profile of SEPs at the Sun and the characteristics (mean free path) of their transport in the interplanetary medium is inverted from 1 AU spacecraft measurements.

In what follows we review first the two inversion approaches used so far and then describe the HESPERIA approach.

10.4.1 Inversion of Spacecraft Data to the Sun

Numerical simulations of the propagation of SEPs along the IMF are a useful tool to understand SEP events and their sources. We currently have a good theoretical understanding of the transport processes that affect SEPs in the interplanetary medium (see Chap. 4). In Sect. 10.3.1 we discussed a model that simulates the processes undergone by SEPs during their propagation from their source to the observer with the critical parameters summarized in the gray box on page 186.

The approach introduced by Agueda et al. (2008) is to utilize the computed response of the "system" to an impulsive (delta) injection at the Sun, i.e. the Green's function of particle transport. A convolution of some delta injections allows us to compute different pitch angle dependent proton intensity time profiles that are used as input to the second step in the chain (see Sect. 10.3.2).

Given a system impulse response, $g(t)$, and the input injection profile $q(t)$, the output, $I(t)$, is the convolution of $g(t)$ and $q(t)$:
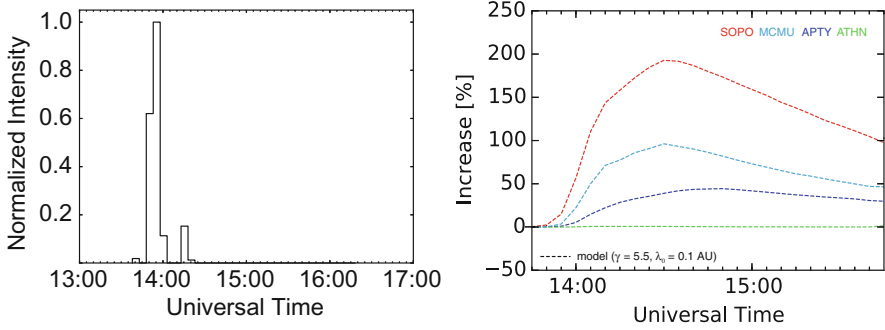
$$I(t) = \int_0^\infty g(t')q(t-t')dt' \qquad (10.4)$$

Fig. 10.3 Convolution of different δ-injections close to the Sun on April 15, 2001 (GLE60) from 13:45 h to 14:15 h (*left panel*) with a set of δ injection $\gamma = 5.5$ at the Sun, and a mean free path $\lambda = 0.1$ AU in interplanetary space leads to intensity increases at the Apatity, Athens, McMurdo and South Pole NM (*right panel*)

i.e., $I(t)$ is the sum of responses resulting from a series of impulses at the Sun, weighted and shifted in time according to $q(t)$. For simplicity, here we assumed that the response is only time-dependent, but the same holds if one includes the energetic and directional dependence in the Green's function.

Particle intensities measured in the heliosphere as a function of time, energy and direction, are obtained as a temporal convolution of the source function (particle injection profile) and the Green's function of particle transport at the spacecraft location. The origin of SEP events can be unfolded by solving the inverse problem (deconvolving the in-situ measurements). The measurements are used to infer the values of the model parameters. It is a deductive approach, and it has the advantage that a systematic exploration of the parameters' space is possible. A simulated GLE time profile with a proton injection from 13:45 h to 14:15 h at the Sun as displayed in the left panel of Fig 10.3 leads to a proton event observable close to Earth by intensity increases at Apatity, Athens, McMurdo and the South Pole displayed in the right panel. A convolution of a δ-injection with $\gamma = 5.5$, and a mean free path $\lambda_0 = 0.1$ AU has been used.

Let's consider an arbitrary function $q(t)$—to be determined—that represents the injection function of SEPs close to the Sun. The modeled directional intensities, M_j^k, resulting from a series of impulse solar injections can be written as

$$M_j^k(t; \lambda) = \int_{T_1}^{T_2} dt' g_j^k(t, t'; \lambda) \, q(t'), \qquad (10.5)$$

where $g_j^k(t, t'; \lambda)$ represents the impulse response in a given direction j and energy interval k, at a given time t, when particle injection took place at time t' and assuming an interplanetary mean free path λ. The duration of the injection function, $t' \in [T_1, T_2]$, is determined by the SEP event time interval selected for fitting, $t \in [t_1, t_2]$, that is, $T_1 = t_1 - \Delta t$ and $T_2 = t_2 - \Delta t$, where Δt is the transit time of the first arriving particles at the spacecraft location, assuming a given value of the scattering

mean free path. The number of time points in the event time interval selected for fitting is equal to $n_t = (t_2 - t_1)/\delta t + 2$, where δt is the time resolution of the data.

Taking discrete values of time, we have

$$M_j^k(t_h; \lambda) = \sum_{l=1}^{n_t} g_j^k(t_h, t_l'; \lambda) \, q(t_l') \tag{10.6}$$

where $j = 1, 2, \ldots, n_s$ are numbers representing the directions (sectors or bins) observed by the telescope, $k = 1, 2, \ldots, n_c$ numbers for the energy channels and $h = 1, 2, \ldots, n_t$ numbers of the time intervals.

Equation (10.6) can be written as

$$M_j^k(t_h; \lambda) \equiv M_i(\lambda) = \sum_{l=1}^{n_t} g_{il}(\lambda) \, q_l = (\mathbf{g} \cdot \mathbf{q})_i \tag{10.7}$$

where $i = k + (j-1) \cdot n_t = 1, 2, \ldots, n_T$ numbers the total number of observational points and $n_T = n_t \, n_s$ gives the total number of observational points in all sectors; $\mathbf{g}$ is an $n_T \times n_t$ matrix with $(\mathbf{g})_{il} = g_{il}(\lambda)$.

In matrix form,

$$\begin{pmatrix} M_1 \\ M_2 \\ \vdots \\ M_{n_T} \end{pmatrix} = \begin{pmatrix} g_{11} & g_{12} & \cdots & g_{1n_t} \\ g_{21} & g_{22} & \cdots & g_{2n_t} \\ \vdots & \vdots & \ddots & \vdots \\ g_{n_T 1} & g_{n_T 2} & \cdots & g_{n_T n_t} \end{pmatrix} \cdot \begin{pmatrix} q_1 \\ q_2 \\ \vdots \\ q_{n_t} \end{pmatrix} \tag{10.8}$$

The goal is to compare the modeled intensities with the observations. Let J_i be the observations (background subtracted). We want to derive the n_t-vector $\mathbf{q}$ that minimizes the length of the vector $\mathbf{J} - \mathbf{M}$, that means minimizing the value of

$$||\mathbf{J} - \mathbf{M}|| \equiv ||\mathbf{J} - \mathbf{g} \cdot \mathbf{q}||, \tag{10.9}$$

subject to the constraint that $q_l \geq 0 \;\; \forall l = 1, 2, \ldots, n_t$. Thus, the best-fit $\mathbf{q} = (q_1, q_2, \ldots, q_{n_t})$ corresponds to a combination of delta-function injection amplitudes. To obtain the best-fit values, we use the NNLS method developed by Lawson and Hanson (1974), which always converges to a solution.

Note, that if each energy channel is fitted separately, the total number of observational points considered in the fit is $n_t n_s$ and the total number of independent fitting parameters (injection amplitudes) is n_t. Since $n_t n_s \gg n_t$, the number of degrees of freedom is clearly much larger than the number of model parameters and the inversion problem is well constrained. If one instead neglects the directional information in the data and uses the modeled omnidirectional intensities to fit the omnidirectional event, then the number of observational points and the number of independent fitting parameters is equal, and the problem is not well constrained (multiple injections and transport scenarios can provide an explanation for the data).

The goodness of fit describes how well the model predictions fit a set of observations. One way to evaluate the goodness of the fit, in case the measurement errors are known, is to construct a weighted sum of squared residuals (for details see Agueda 2008). The χ^2 estimator does not work very well for SEP events because during impulsive events the maximum intensities can be several orders of magnitude higher than the intensities observed during the decay phase, thus emphasizing the peak period. Therefore a better goodness-of-fit estimator is provided by the sum of the squared logarithmic differences between the observational and the modeled data. This estimator gives an equal weight of all relative residuals instead of just emphasizing the goodness of fit at the time of maximum. By evaluating the goodness of the fit under different interplanetary transport conditions (different values of λ), one can objectively discern the "best fit" scenario (λ-value and associated injection profile) by minimizing the values of the goodness-of-fit estimator.

10.4.2 Inversion of NM Data to the Border of the Earth's Magnetosphere

In general, the standard analysis of GLE events is based on an inverse problem, where data by the worldwide network of NMs is used to determine the spectral and angular characteristics of SEPs near Earth causing GLEs for selected times (Shea and Smart 1982; Mishev et al. 2014). Analysis of the characteristics of the primary solar particles causing GLEs from ground-based data records is a serious challenge (Bütikofer and Flückiger 2013). Data from stations with different cutoff rigidities (geomagnetic latitudes) provide information necessary to determine the spectral characteristics. Responses of stations over a wide range of geographical locations are required to determine the axis of symmetry. Data are fitted to directional distributions that are rotationally symmetric about one direction in space. This, in principle, is close but not exactly the direction of the instantaneous magnetic field measured close to the Earth but outside the Earth's magnetosphere (Bieber et al. 2013). Therefore, axis-symmetry is assumed, but the direction of the axis of symmetry is optimized to fit the data.

The PADs of relativistic solar protons in space are assumed to follow a given functionality. A variety of functions has been used in the literature. These include a linear form, an exponential plus a constant, a parabola, two Gaussians, and two exponentials plus constant. The latter three are expected to provide better fits to bidirectional fluxes, if present (Bieber et al. 2013; Mishev et al. 2014).

Similarly, the spectra of relativistic solar protons during a GLE are assumed to follow a power law in rigidity, or energy with extensions that describe the softening of the spectrum at higher energies by multiplying a power law with an exponential cutoff.

The parameters of the rigidity spectrum, the PAD and the direction of symmetry are determined by minimizing the sum of squared differences between the modeled relative change in the NM count rate at the station x

$\left(\frac{\Delta N_x}{N_x}\right)_{\text{mod.}}$ and
the corresponding observed relative count rate change
$\left(\frac{\Delta N_x}{N_x}\right)_{\text{obs.}}$

$$F = \sum_{x=1}^{m} \left[\left(\frac{\Delta N_x}{N_x}\right)_{\text{mod.}} - \left(\frac{\Delta N_x}{N_x}\right)_{\text{obs.}} \right]^2 \qquad (10.10)$$

for the set of selected NM data. The Levenberg-Marquardt algorithm (LMA) (Marquardt 1963) provides a numerical solution to the problem of minimizing a nonlinear function over the space of parameters of the function. The goodness of the fit is commonly expressed by a weighted sum of squared residuals or by computing a correlation coefficient, ρ between measurements and the model.

10.4.3   The HESPERIA Approach

For the first time, models of the transport of SEPs in the interplanetary medium, the Earth's magnetosphere and atmosphere, and the response of NMs are linked to each other. The first goal is to compute the expected additional count rate, N, caused by SEP for a given NM station, based on the intensities of the primary cosmic rays near Earth, $I(R, \alpha, t)$, as function of rigidity, R, pitch angle, α, and time, t. As detailed above the interplanetary transport is described by Green's functions representing characteristics of the SEP interplanetary transport conditions. To ascribe the magnetospheric transport, the magnetic field direction outside the magnetosphere is computed from interplanetary measurements, and the asymptotic directions are calculated utilizing the PLANETOCOSMICS code in GSE coordinates. The latter can be found at the HESPERIA webpage during each GLE in the past and for the NMs of the worldwide network.

Since the parameters are the same than the ones used by Agueda et al. (2008) the differences lie in the indirect measurement of the pitch angle dependent count rate and the integration over wide energy ranges: For all NM stations, the counting rate increases can then be computed for a series of delta injections from the Sun and for selected times. Note that the hardness of the source spectra described by γ is assumed to be constant in the HESPERIA approach for all δ-injections. The amplitudes of the source components, for a given scenario, are inferred by fitting the NM observations with the modeled NM counting rate increases. The NNLS algorithm described in Sect. 10.4.1 is used to determine the best set of parameters. Regularized inversion approaches will be explored for refinements. The goodness of the fit will be evaluated by computing a weighted sum of the squared residuals.

The result of the inversion problem is a detailed time profile of the injection process at the Sun. The shape of this profile is presumably determined by details of the acceleration process and possible transport processes in the corona (see Chap. 3 for details).

In contrast to a classical approach with a total number of at least 10 fit parameters to derive the injection function at the Sun (see Sect. 10.4.2) the HESPERIA approach relies on several well-documented assumptions (see Chaps. 3, 4, and 5) reducing the number of free parameters. Assuming for each rigidity a number of delta injection at the source region the phase space density $f(z, \mu, t)$ close to Earth can be calculated for any given time t corresponding to the distance $z(v)$ that depends on the measured solar wind velocity v. The mean free path λ_0, the number of particles, the injection time profile and its rigidity spectrum described by a power law with index γ are utilized to derive $f(z, \mu, t)$. The cosmic ray particle trajectories through the Earth's magnetosphere are computed for selected rigidities R_c, $R_c + 0.1$ GV ...20 GV as a function of GSE coordinates of the NM station, for a selected time. Applying the Tsyganenko 1989 (Tsy89) model and the yield function for each NM we can ascribe the SEP time profiles for the NM network by a minimum of free parameters.

10.5   Results and Validation

Since the HESPERIA approach depends on the knowledge of the IMF outside the Earth's magnetosphere that is provided by OMNI since November 4, 1973, our investigation is restricted to GLEs with numbers larger than number 26 occurring on April 30, 1976. To validate the results, pitch angle dependent intensity time profiles of protons with energies above 500 MeV are needed. Here we utilize SOHO/EPHIN and Wind 3DP measurements. The latter are needed in order to estimate the pitch angle coverage of SOHO/EPHIN.

Since SOHO was launched in December 1995, we restrict our validation to GLEs with numbers ≥55 (GLE55 occurred on November 6, 1997). Kühl et al. (2015, 2016) showed that EPHIN is capable of measuring the proton spectra in the range from 100 MeV to above 1 GeV. Since no magnetic field measurements are available on SOHO, we compare the intensity-time-profiles of near relativistic electrons measured by EPHIN and Wind 3DP with each other. In Fig. 10.4 different colored curves show the pitch angle dependent time-profiles for Wind 3DP with energies between 230 and 646 keV. Three thick black lines show the EPHIN measurements with energies between 0.25 and 0.7 MeV multiplied by different factors (0.05, 0.08, and 0.1 as solid, dashed, and dashed-dotted lines) to take into account cross
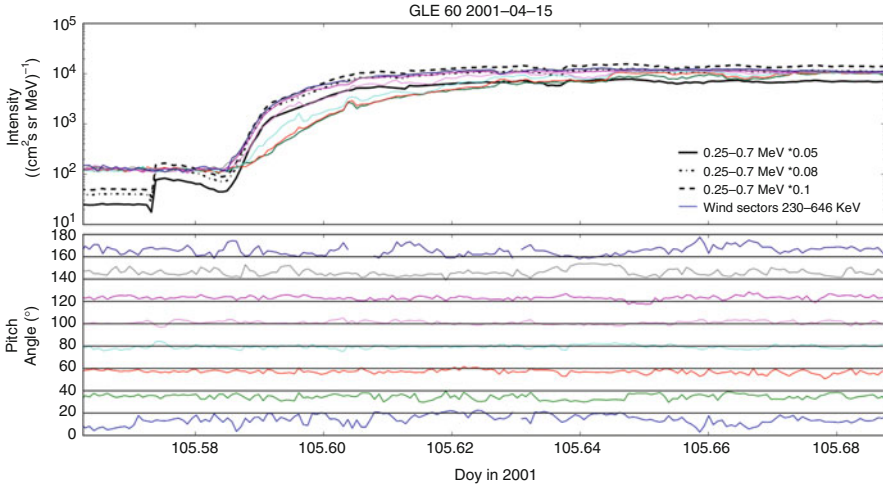
Fig. 10.4 *From top to bottom:* Hourly averaged intensity time profiles of 234–646 keV electrons measured by Wind 3DP. The different colors give the pitch angle coverage for the WIND observations shown in the *bottom panels*. Also the *solid, dashed and dashed-dotted lines* represent the 0.25–0.7 MeV EPHIN electron measurements multiplied by a factor 0.05, 0.08, and 0.1 respectively

calibration. Only the dashed-dotted line agrees with all Wind sectors when the flux becomes isotropic. Thus we assume that the curve that agrees best with the dashed-dotted line ascribes the viewing direction of EPHIN. In our example, the purple curve describing the measurements at a pitch angle of 120° fulfills this criteria best.

Figure 10.5 is an extension of Fig. 10.3 that only showed predicted intensity time profiles close to Earth and by different NMs. It compares the results computed with the GLE inversion software with measurements of other facilities as radio telescopes, NMs and particle detectors in space. The parameters used in the prediction were derived by the inversion of the NM data for GLE 60. The middle panel of Fig. 10.5 compares the simulated and measured intensity time profiles of the Apatity, Athens, McMurdo and South Pole NMs with each other showing a good agreement between measurements and the model. The injection profile close to the Sun is shown in the left panel together with the micro wave profile measured by the Radio Solar Telescope Network (RSTN) showing a good agreement between the particle component injected into interplanetary space and towards the lower corona. Note, that the injection profile is in very good agreement with the one derived by Bieber et al. (2004). For details on micro waves and their importance, the reader is referred to Chap. 2.

The middle bottom panel displays the energy spectrum between 100 MeV and 1 GeV predicted by the model (red curve) and measured by EPHIN (black curve). Note, that the prediction was scaled down by a factor of ∼20. From the figure, it is evident that the model predicts the same spectral index when taking into account the contribution of electrons at 900 and 700 MeV, respectively (for details see Kühl et al. 2017).
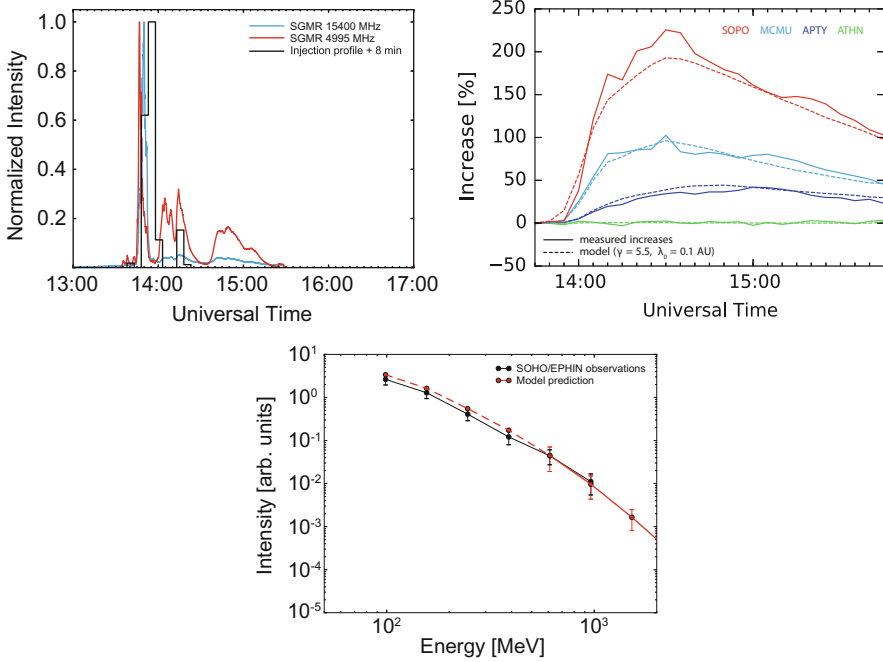
Fig. 10.5 Predicted δ-injections (*upper left panel*), NM increases (*upper right panel*) and differential intensity spectrum (*lower panel*) for GLE60 (see also Fig. 10.3) in comparison to actual measurements (for details see text)

10.6 Concluding Remarks

A new approach has been presented here that allows computing the injection function of SEP close to the Sun based on the data of the worldwide NM network during a GLE. This injection function is described by a power law in rigidity R with two parameters that are the intensity at $R_0 = 1$ GV and the spectral index γ. For the interplanetary transport, we utilize a 1-dimensional model with the mean free path λ_r as free parameter. The solar wind speed taken from interplanetary measurements determines the length of the magnetic field line connecting the Earth back to the Sun. The IMF direction is taken from the OMNI data set using appropriate accumulation periods. The transport through the Earth's magnetosphere is computed with the PLANETOCOSMICS software using the Tsy89 model for the outer Earth's magnetic field. The NM yield function describes the passage of the cosmic ray particles through the atmosphere and the detection of the secondary nucleon component by the NMs. Using this model chain GLE 60 could be reproduced very well. A discrepancy between the prediction and the measurements in interplanetary space exists that needs further investigations. Especially the whole number of observed GLEs should be analyzed and validated by using GOES HEPAD data that

go back to the 1970s. Further improvements like utilizing more sophisticated models of the magnetosphere and the interplanetary transport, as well as different NM yield functions, should be taken into account in order to improve the model presented here.

References

Adriani, O., Barbarino, G.C., Bazilevskaya, G.A., Bellotti, R., Boezio, M., Bogomolov, E.A., Bonechi, L., Bongi, M., Bonvicini, V., Borisov, S., et al.: Astrophys. J. **742**, 102 (2011). doi:10.1088/0004-637X/742/2/102

Agueda, N.: Near-relativistic electron events. Monte Carlo simulations of solar injection and interplanetary transport. Ph.D. thesis, Dep. Astronomia i Meteorologia University of Barcelona Martí i Franquès 1 08028 Barcelona (2008)

Agueda, N., Vainio, R., Lario, D., Sanahuja, B.: Astrophys. J. **675**, 1601 (2008). doi:10.1086/527527

Aguilar, M., Alberti, G., Alpat, B., Alvino, A., Ambrosi, G., Andeen, K., Anderhub, H., Arruda, L., Azzarello, P., Bachlechner, A., et al.: Phys. Rev. Lett. **110**(14), 141102 (2013). doi:10.1103/PhysRevLett.110.141102

Agueda, N., Klein, K.L., Vilmer, N., Rodríguez-Gasén, R., Malandraki, O.E., Papaioannou, A., Subirà, M., Sanahuja, B., Valtonen, E., Dröge, W., et al.: Astron. Astrophys. **570**, A5 (2014). doi:10.1051/0004-6361/201423549

Aschwanden, M.J.: Space Sci. Rev. **171**, 3 (2012). doi:10.1007/s11214-011-9865-x

Bieber, J.W., Evenson, P., Dröge, W., Pyle, R., Ruffolo, D., Rujiwarodom, M., Tooprakai, P., Khumlumlert, T.: Astrophys. J. Lett. **601**, L103 (2004). doi:10.1086/381801

Bieber, J.W., Clem, J., Evenson, P., Pyle, R., Sáiz, A., Ruffolo, D.: Astrophys. J. **771**, 92 (2013). doi:10.1088/0004-637X/771/2/92

Bütikofer, R., Flückiger, E.O.: J. Phys. Conf. Ser. **409**(1), 012166 (2013). doi:10.1088/1742-6596/409/1/012166

Cliver, E.W., Kahler, S.W., Reames, D.V.: Astrophys. J. **605**, 902 (2004). doi:10.1086/382651

Dalla, S., Marsh, M.S., Kelly, J., Laitinen, T.: J. Geophys. Res. (Space Phys.) **118**, 5979 (2013). doi:10.1002/jgra.50589

Dalla, S., Marsh, M.S., Laitinen, T.: Astrophys. J. **808**, 62 (2015). doi:10.1088/0004-637X/808/1/62

Dresing, R., Gómez-Herrero, N., Klassen, A., Heber, B., Kartavykh, Y., Dröge, W.: Sol. Phys. **281**, 281 (2012). doi:10.1007/s11207-012-0049-y

Dresing, N., Gómez-Herrero, R., Heber, B., Klassen, A., Malandraki, O., Dröge, W., Kartavykh, Y.: Astron. Astrophys. **567**, A27 (2014). doi:10.1051/0004-6361/201423789

Dröge, W.: Astrophys. J. **537**, 1073 (2000). doi:10.1086/309080

Dröge, W.: Astrophys. J. **589**, 1027 (2003). doi:10.1086/374812

Dröge, W., Kartavykh, Y.Y., Klecker, B., Kovaltsov, G.A.: Astrophys. J. **709**, 912 (2010). doi:10.1088/0004-637X/709/2/912

Gold, R.E., Krimigis, S.M., Hawkins, S.E.I., Haggerty, D.K., Lohr, D.A., Fiore, E., Armstrong, T.P., Holland, G., Lanzerotti, L.J.: Space Sci. Rev. **86**(1), 541 (1998)

Hasselmann, K., Wibberenz, G.: Astrophys. J. **162**, 1049 (1970)

Kartavykh, Y.Y., Dröge, W., Klecker, B., Mason, G.M., Möbius, E., Popecki, M., Krucker, S.: Astrophys. J. **671**, 947 (2007). doi:10.1086/522687

Klecker, B.: J. Phys. Conf. Ser. **409**(1), 012015 (2013). doi:10.1088/1742-6596/409/1/012015

Klein, K.L., Trottet, G.: Space Sci. Rev. **95**, 215 (2001)

Kounine, A.: Int. J. Modern Phys. E **21**(08), 1230005 (2012). doi:10.1142/S0218301312300056. http://www.worldscientific.com/doi/abs/10.1142/S0218301312300056

Kühl, P., Banjac, S., Dresing, N., Goméz-Herrero, R., Heber, B., Klassen, A., Terasa, C.: Astron. Astrophys. **576**, A120 (2015). doi:10.1051/0004-6361/201424874

Kühl, P., Dresing, N., Heber, B., Klassen, A.: Solar energetic particle events with protons above 500 MeV between 1995 and 2015 measured with SOHO/EPHIN. Sol. Phys. **292**(10), 10 (2017). arXiv:1611.03289. doi:10.1007/s11207-016-1033-8. http://adsabs.harvard.edu/abs/2017SoPh.. 292...10K

Kühl, P., Dresing, N., Heber, B., Klassen, A.: Sol. Phys. **292**, 10 (2017). doi:10.1007/s11207-016-1033-8

Lawson, C.L., Hanson, R.J.: Solving Least Squares Problems. SIAM, Philadelphia (1974)

Lin, R.P., Anderson, K.A., Ashford, S., Carlson, C., Curtis, D., Ergun, R., Larson, D., McFadden, J., McCarthy, M., Parks, G.K., et al.: Space Sci. Rev. **71**, 125 (1995). doi:10.1007/BF00751328

Linsley, J.: Phys. Rev. **97**, 1292 (1955). doi:10.1103/PhysRev.97.1292

Marquardt, D.W.: J. Soc. Ind. Appl. Math. **11**(2), 431 (1963). doi:10.1137/0111030

Mason, G.M.: Space Sci. Rev. **130**, 231 (2007). doi:10.1007/s11214-007-9156-8

Mason, G.M., Mazur, J.E., Looper, M.D., Mewaldt, R.A.: Astrophys. J. **452**, 901 (1995). doi:10.1086/176358

McCracken, K.G., Moraal, H., Shea, M.A.: Astrophys. J. **761**, 101 (2012). doi:10.1088/0004-637X/761/2/101

McDonald, F.B.: Phys. Rev. **104**, 1723 (1956). doi:10.1103/PhysRev.104.1723

Mewaldt, R.A., Cohen, C.M.S., Mason, G.M., Cummings, A.C., Desai, M.I., Leske, R.A., Raines, J., Stone, E.C., Wiedenbeck, M.E., von Rosenvinge, T.T., et al.: Space Sci. Rev. **130**, 207 (2007). doi:10.1007/s11214-007-9187-1

Mewaldt, R.A., Looper, M.D., Cohen, C.M.S., Haggerty, D.K., Labrador, A.W., Leske, R.A., Mason, G.M., Mazur, J.E., von Rosenvinge, T.T.: Space Sci. Rev. **171**, 97 (2012). doi:10.1007/s11214-012-9884-2

Meyer, P., Evenson, P.: IEEE Trans. Geosci. Electron. **16**, 180 (1978)

Mishev, A.L., Kocharov, L.G., Usoskin, I.G.: J. Geophys. Res. **119**, 670 (2014). doi:10.1002/2013JA019253

Moraal, H., Caballero-Lopez, R.A.: Astrophys. J. **790**, 154 (2014). doi:10.1088/0004-637X/790/2/154

Moraal, H., McCracken, K.G.: Space Sci. Rev. **171**, 85 (2012). doi:10.1007/s11214-011-9742-7

Müller-Mellin, R., Kunow, H., Fleißner, V., Pehlke, E., Rode, E., Röschmann, N., Scharmberg, C., Sierks, H., Rusznyak, P., McKenna-Lawlor, S., et al.: Sol. Phys. **162**(1), 483 (1995)

Nitta, N.V., Mason, G.M., Wang, L., Cohen, C.M.S., Wiedenbeck, M.E.: Astrophys. J. **806**, 235 (2015). doi:10.1088/0004-637X/806/2/235

Picozza, P., Galper, A.M., Castellini, G., Adriani, O., Altamura, F., Ambriola, M., Barbarino, G.C., Basili, A., Bazilevskaja, G.A., Bencardino, R., et al.: arXiv.org (4), 296 (2006)

Reames, D.V.: Space Sci. Rev. **90**, 413 (1999). doi:10.1023/A:1005105831781

Rinehart, M.C.: Nucl. Inst. Methods **154**, 303 (1978). doi:10.1016/0029-554X(78)90414-7

Roelof, E.C.: Propagation of solar cosmic rays in the interplanetary magnetic field. In: Ögelman, H., Wayland, J.R. (Eds.) Lectures in High-Energy Astrophysics, p. 111 (1969). http://adsabs.harvard.edu/abs/1969lhea.conf..111R. Provided by the SAO/NASA Astrophysics Data System

Rouillard, A.P., Odstrecil, D., Sheeley, N.R., Tylka, A., Vourlidas, A., Mason, G., Wu, C.C., Savani, N.P., Wood, B.E., Ng, C.K., et al.: Astrophys. J. **735**, 7 (2011). doi:10.1088/0004-637X/735/1/7

Sauer, H.H.: Int. Cosmic Ray Conf. **3**, 250 (1993)

Shea, M.A., Smart, D.F.: Space Sci. Rev. **32**, 251 (1982). doi:10.1007/BF00225188

Simpson, J.A.: Phys. Rev. **73**, 1389 (1948). doi:10.1103/PhysRev.73.1389

Tylka, A.J., Cohen, C.M.S., Dietrich, W.F., Lee, M.A., Maclennan, C.G., Mewaldt, R.A., Ng, C.K., Reames, D.V.: Astrophys. J. **625**, 474 (2005). doi:10.1086/429384

Wiedenbeck, M.E., Mason, G.M., Cohen, C.M.S., Nitta, N.V., Gómez-Herrero, R., Haggerty, D.K.: Astrophys. J. **762**, 54 (2013). doi:10.1088/0004-637X/762/1/54